

RESEARCH PAPER

Predictive Digital Mapping of Surface Soil Properties using Remote Sensing and Multivariate Statistical Analysis.

Kwestan O. Abdalkarim¹, Heman Abdulkhaleq A. Gaznayee^{2*}, Ayad M. F. Al-Quraishi³, Zhino O. Abdalla¹.

¹Department of Natural Resource, College of Agricultural Engineering Sciences, Sulaimaniyah University, Sulaimaniyah, Kurdistan Region, Iraq

²Department of Forestry, College of Agricultural Engineering Sciences, Salahaddin University, Erbil, Iraq - Erbil 44003, Kurdistan Region, Iraq

³Petroleum and Mining Engineering Department, Faculty of Engineering, Tishk International University, Erbil, 44001, Kurdistan Region, Iraq

ABSTRACT:

Accurate prediction of surface soil properties is crucial for agricultural and environmental purposes. This study aimed to utilize geoinformatics approaches and Landsat OLI-8 data to predict specific physicochemical properties of the surface soil in Sulaimaniyah, Kurdistan Region of Iraq (KRI). It also examined the statistical relationships between these properties and spectral reflectance, vegetation cover, soil/vegetation moisture contents, and elevation. The study made use of the Normalized Difference Vegetation Index (NDVI) and Normalized Difference Moisture Index (NDMI), as well as seven bands of the OLI image for the statistical analysis. The results demonstrated a statistical connection between organic matter (O.M.) and vegetation cover based on NDVI. It was observed that the northern parts of Sulaimaniyah exhibited dense vegetation, albeit covering a small area. Generally, mountainous regions had a higher proportion of canopy cover compared to other parts of the arid zone, with moisture availability being the most influential factor on vegetation. Moreover, the majority of the research area showed the highest CaCO₃ content and a significant negative relationship was found between vegetation (NDVI) and soil moisture (NDMI) with organic matter (O.M.) and clay. Using geoinformatics datasets and techniques proved valuable in identifying, mapping, and investigating specific surface physicochemical properties in the study area.

KEY WORDS: Landsat 8-OLI, Sulaimaniyah, Soil Map, Spectral response, Surface soil properties.

DOI: <http://dx.doi.org/10.21271/ZJPAS.35.6.19>

ZJPAS (2023) , 35(6);189-203

1. INTRODUCTION :

Methods for rapid and accurate determination of physicochemical soil properties are vital for quantitative land management assessments and ecological modeling studies (Nawar et al., 2015). Soil analyses are expensive, and dense sampling is obligatory to sufficiently characterize the spatial variability of an area, making broad-scale quantitative evaluation hard (Lutes et al., 2006).

Furthermore, the traditional method of soil analysis and interpretation by chemical treatment is costly, time-consuming, and environmentally damaging, mainly when the survey is performed on a national, regional, or global scale (Vaudour et al., 2015). Geo-informatics is a modern discipline of science that integrates the acquisition, modeling, analysis, and management of spatially referenced data. The majority of Geo-informatics involves the application of Remote Sensing (RS), Geographical Information Systems (GIS), and Global Positioning System (GPS) technologies

* Corresponding Author:

Heman Abdulkhaleq A. Gaznayee

E-mail: heman.ahmed@su.edu.krd

Article History:

Received:13/03/2023

Accepted: 05/06/2023

Published: 15/12 /2023

(Senanayake *et al.*, 2020). It is vital to map soil properties with effective tools, and the GIS has been one of the most useful tools throughout the twenty-first century. In GIS, numerous interpolation techniques are available. These methods generate new data points within the range of a discrete set of known data points gathered by field sampling. Consequently, it is possible to produce raster or grid maps for soil properties using various interpolation methods in GIS (Eskandari Dameneh *et al.*, 2021).

GIS permits several modifications, such as map measurers, map overlay changes, geographic design, and database management (Nanni *et al.*, 2012). GPS is a space-based system that provides accurate location and time information in all-weather situations, at all times, wherever on or near Earth, when and where there is a clear line of sight to at least four GPS satellites. It offers locational information (latitude, longitude, and elevation). On the other hand, technological developments in remote sensing picture acquisition enable the collection of high-resolution images, which help determine soil characteristics, monitoring degradation, and estimating natural resource availability (soil, vegetation, and water bodies).

Remote sensing depends on observing spectral changes in the energy reflected or emitted by objects or features on Earth. In other words, remote sensing aids researchers in their search for variations in the reflected energy of objects (Wodaje, 2016), which is the origin of multispectral remote sensing (Kercival, 2015). Remote sensing data is an unequalled source of consistent spatial data for experts, while GIS permits the modeling and creation of more precise maps. Therefore, it is vital to investigate the potential relationships between soil characteristics and satellite image digital number (DN) values. It has been investigated as an alternate method for determining soil parameters (Hartemink, 2016; Hayes and Cohen, 2007; Nawar *et al.*, 2015). Remote sensing provides unique capabilities for deep insight essential for analyzing, making decisions, and regulating environmental processes. Experimental models are crucial for associating field-measured variables to remotely sensed data, and regression analysis is a common empirical method for integrating these two forms of data to generate continuous estimates of environmental variables (Vicente Barros and Christopher B.

Field, 2012). Several studies have demonstrated that maps of mineral composites, such as ferrous minerals, iron oxide, and clay minerals, may be created using GIS, Landsat-7 ETM+ images, and indices (Dogan 2008, 2009). Other studies, such as (Abuelgasim and Ammad, 2019; Shabou *et al.*, 2015), have also built models for predicting soil properties from spectral data, finding a quantitative correlation, and employing field and laboratory instruments. Iraq is one of the Middle East's most significant agricultural product-consuming nations, mainly for wheat, rice, vegetables, and fruits.

Therefore, to boost the local agricultural industry, proper land use planning is required (Razvanchy, 2008). A database for soil characteristics and features is essential to agricultural planning. Traditional soil analyses have played a vital role in the soil evaluation process as part of the soil evaluation procedure (Nawar *et al.*, 2015). Current procedures include excavating holes, collecting soil samples, and preparing them for chemical and physical laboratory analysis, but this method for analyzing soil samples is expensive, time-consuming, relatively slow, and produces chemical waste that must be discarded. The electromagnetic radiation (EMR) that strikes the earth's surface interacts with objects and is reflected, absorbed, and/or transmitted in proportion to their physical, chemical, and biological properties (Akbari *et al.*, 2021). Several elements, including particle size, soil structure, water content, surface rugosity, organic matter content, carbonate-based minerals, quartz, and iron oxides, contribute to the soil's spectral reflectance. Several soil characterization techniques utilizing soil reflectance have been developed (Al-Quraishi *et al.*, 2019).

Due to the availability of more efficient and cost-effective technology, soil spectral characterization is now widely employed. Despite this, soil detection, categorization, and discrimination are the most common applications of this approach (Qader *et al.*, 2021). Using spectral analysis to assess soil's chemical and physical characteristics has received little attention, and there are distinctions between laboratory data and remote sensing data. Nevertheless, a few inconclusive experiments assess soil characteristics using satellite sensor-based information. The remotely sensed data reduces atmospheric and geometric interference

(Red, 2006; Yaghoobi and Zargar, 2012). The aim of this study:

The general objective of this study is to setup a relationship between the soil spectral properties (Landsat-8 images reflectance with the chemical and physical characteristics of the soils for some sites in the Iraqi Kurdistan region. The specific objectives are to:

1. Estimating the statistical relationships among the spectral soil properties (using the Landsat-8 images and Spectroradiometer reflectance), chemical, and physical characteristics for the soil samples of the study area.
2. Predicting some of the chemical and physical characteristics of the soil in the study area.

2. MATERIALS AND METHODS

2.1. THE STUDY AREA

Sulaymaniyah, situated in northeastern Iraq, is the largest governorate within the KRI. It shares its borders with Iran and is located at geographic coordinates $35^{\circ}33'40''$ N and $45^{\circ}26'14''$ E. The governorate comprises ten districts, with the center of Sulaymaniyah itself situated at an elevation of approximately 830 meters above sea level. To the north, west, and south of Sulaymaniyah, four Iraqi governorates border it, namely Erbil, At-Ta'mim, Salah ad-Din, and Diyala. The study area (Fig. 1) comprises all of Sulaimaniyah Governorate, comprising 15 districts: Sulaimaniyah, Qaradagh, Sharazure, Saidaadiq, Penjwin, Halabja, Darbandikhan, Kalar, Khanaqin, Kifri, Chamchamal, Dukan, Sharbazher (Mawat), Ranya, and Pishdar. The study area is bordered on the east by Iran, the west by Kirkuk Governorate, the southwest by Salahalddin Governorate, and the south by Diyala Governorate.

2.1.1 Physiography of the study area

The KRI mountains are within the larger Zagros Mountains range, extending into Iran. These mountains are characterized by their fertile plains, plentiful water sources, and picturesque scenery, with several rivers traversing the region. The Great and Little Zab rivers flow from east to west, adding to the distinctiveness of this area. In contrast to the eastern part, the western and southern regions of the KRI display a relatively

smoother topography, featuring rolling hills and sporadic flat plains (Razvanchy, 2008).

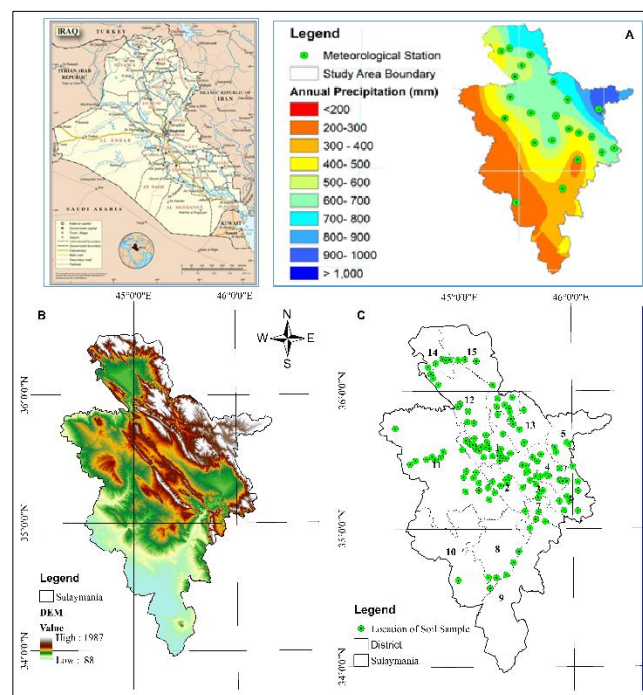


Fig1: Location map of the study area in the KRI. (A); The map of the meteorological stations and the geographical distribution of annual rainfall (mm/year) in Sulaymaniyah for 24 years (B); Digital Elevation Model (DEM); and(C) Location map of soil sample District numbers: 1, Sulaimaniyah; 2, Qaradagh; 3, Sharazure; 4, Saidaadiq; 5, Penjwin; 6, Halabja; 7, Darbandikhan; 8, Kalar; 9, Khanaqin; 10, Kifri; 11, Chamchamal; 12, Dukan; 13, Sharbazher (Mawat); 14, Ranya; 15, Pishdar.

2.1.2 Climate of the study area

In general, the climate of the studied region is characterized by harsh conditions with considerable temperature variations between day and night and winter and summer. In the summer, the daily temperature at the southern boundaries of the governorates exceeds 45°C . At night, temperatures fall below 20°C in the northern regions, and winter daytime temperatures range from approximately -15°C to approximately 15°C . Accordingly, the climate of the study area has been designated as continental semiarid. In other words, summer is hot and dry, whereas winter is chilly and wet. Spring and fall have shorter seasons than summer and winter (Al-quraishi and Negm, 2019).

Table (1) The monthly air averages temperature in Sulaimaniyah for the years (2000-2020).

YEARS	Months											
	Jan	Feb	Mar	Apr	May	Jun	Jul	Aug	Sep	Oct	Nov	Dec
2000	9.5	16.6	18.5	30.2	38.9	47.8	56.6	52.9	44.5	36.8	23.0	14.4
2001	12.4	15.1	24.5	28.7	36.6	48.4	53.0	52.5	45.8	40.2	21.6	14.2
2002	9.0	15.7	22.8	24.5	36.7	46.4	51.7	49.9	45.6	40.8	23.9	11.1
2003	11.4	11.3	16.7	27.8	38.6	46.7	51.6	53.3	44.2	39.8	22.2	13.8
2004	11.2	12.8	24.5	26.7	34.2	46.3	51.0	50.6	46.6	40.5	20.2	12.4
2005	10.3	11.5	22.0	30.1	39.0	47.3	54.4	51.7	47.5	38.7	23.9	20.2
2006	9.3	14.3	24.1	30.0	38.4	49.9	51.7	55.6	45.7	40.1	21.6	13.2
2007	9.7	15.1	23.2	24.8	41.6	48.9	52.3	52.3	47.6	42.1	25.3	15.3
2008	7.0	13.2	28.0	35.2	38.8	48.0	53.4	55.1	46.5	39.5	23.7	16.4
2009	11.9	17.0	20.4	26.5	38.8	46.9	51.7	50.7	42.4	37.3	21.9	16.6
2010	14.9	17.5	24.5	28.8	37.5	49.6	54.1	54.9	49.6	41.7	29.0	20.3
2011	10.9	14.1	21.7	28.3	37.1	48.3	54.4	52.6	45.4	37.6	18.5	16.6
2012	10.5	12.8	16.3	32.2	40.1	49.4	53.5	53.8	47.4	41.4	25.7	16.5
2013	12.0	17.9	23.4	31.7	38.0	48.2	53.4	52.4	44.6	36.6	24.5	12.6
2014	12.3	16.2	22.4	29.7	40.1	48.5	53.5	54.4	45.8	38.3	22.3	17.9
2015	13.0	17.4	22.2	29.2	40.6	49.1	56.1	55.8	49.3	41.3	22.7	14.3
2016	11.6	19.3	21.9	29.9	39.0	53.5	54.9	56.4	46.0	38.4	25.1	12.6
2017	11.5	11.4	20.5	29.8	39.7	48.4	55.7	55.6	49.9	39.7	24.3	20.2
2018	13.0	17.6	26.7	30.2	36.7	48.0	54.2	53.2	47.9	41.2	22.4	15.3
2019	11.8	15.2	17.3	24.4	39.5	50.6	52.1	54.5	46.5	40.5	24.7	17.2
2020	12.1	13.5	23.0	28.9	40.1	48.2	55.3	51.5	50.0	41.6	26.1	18.2

Table (2) The monthly rainfall in the study area for the hydrological year (2000-2021)

Years	Location No.														
	1	2	3	4	5	6	7	8	9	10	11	12	13	14	15
1999 -2000	388.4	274.0	396.9	274.0	384.0	393.9	289.6	308.8	268.4	192.9	214.5	379.4	274.0	331.1	325.0
2000 -2001	524.3	550.5	603.7	366.4	693.2	448.3	315.9	317.0	416.0	285.2	416.3	463.1	462.9	616.8	527.6
2001 -2002	782.7	898.2	732.8	738.9	1281.9	851.9	886.1	432.2	485.8	287.4	543.2	721.6	925.5	975.2	985.5
2002 -2003	880.8	924.8	851.6	647.3	1441.1	779.5	783.5	277.5	390.5	173.1	591.9	750.7	914.1	1003.7	1120.7
2003 -2004	852.5	869.3	775.4	648.9	1240.3	943.5	705.0	275.3	346.3	134.3	607.0	877.5	991.7	1044.1	1043.7
2004 -2005	654.5	820.8	713.0	516.1	1074.6	823.8	693.7	322.7	387.3	214.0	560.3	815.7	813.0	879.7	709.7
2005 -2006	747.5	912.8	736.5	737.6	1261.6	873.4	651.7	293.2	250.4	250.1	407.4	656.4	562.6	748.3	705.9
2006 -2007	607.2	731.8	646.3	560.6	1126.1	684.3	486.1	234.7	273.2	234.5	305.4	606.0	762.9	875.5	538.7
2007 -2008	370.4	103.6	201.6	265.0	522.4	297.5	218.1	106.3	139.1	193.7	148.9	224.6	326.2	307.4	360.1
2008 -2009	423.8	353.9	332.2	322.7	655.7	486.5	357.9	214.5	200.2	238.3	249.5	288.5	413.0	389.8	529.1
2009 -2010	799.8	883.5	805.8	707.4	1241.0	880.6	790.4	386.3	507.2	474.4	533.4	564.2	916.5	847.9	773.1
2010 -2011	568.9	607.5	486.8	525.2	928.8	627.7	618.4	246.4	342.3	222.9	361.9	475.7	662.6	663.5	673.0
2011 -2012	548.6	628.8	436.0	435.5	1016.2	592.6	409.0	149.6	203.6	143.2	204.4	421.8	658.9	540.1	635.5
2012 -2013	431.4	697.8	513.1	549.9	1055.5	672.0	630.4	380.6	447.5	258.0	549.7	553.0	772.4	830.4	820.1
2013 -2014	439.6	799.0	568.0	480.3	911.2	485.0	480.4	340.8	412.3	363.2	499.2	449.1	600.9	581.8	699.7
2014 -2015	353.9	733.2	612.2	523.6	910.1	553.8	497.9	283.6	356.2	226.0	481.0	595.1	751.8	673.5	652.7
2015 -2016	765.1	1457.0	854.3	885.2	1443.4	795.9	916.2	558.9	806.1	868.8	709.6	804.2	990.3	941.2	1028.5
2016 -2017	552.8	804.1	541.0	526.7	901.5	506.5	472.6	271.4	300.6	232.8	430.3	518.8	697.6	541.7	572.0
2017 -2018	643.7	1029.0	725.7	566.8	1131.9	534.5	561.2	274.2	391.4	257.8	537.9	659.2	826.9	849.4	863.5
2018 -2019	1147.5	1727.5	1159.6	1159.9	1877.7	1081.4	1338.6	681.8	900.0	608.4	914.3	1041.8	1296.6	1618.4	1374.5
2019 -2020	745.9	1162.8	1209.8	511.8	1025.9	544.1	561.0	367.0	341.0	334.0	582.8	559.6	809.2	931.7	756.0
2020 -2021	378.8	485.5	653.6	307.1	695.5	257.6	238.2	117.5	198.9	115.2	285.2	287.0	478.5	405.9	449.5

Consequently, greater temperature fluctuations were seen between climate station locations (Table 1). Typically, precipitation rises from the southwest to the Northeast. The average yearly precipitation in the study region varied between 450 and 700 mm (Najmaddin *et al.*, 2017). The yearly average precipitation ranges from 350 mm in the Sulaimaniyah region to over 1100 mm in the high mountains bordering Iran (Ahmed and Al-quraishi, 2020). From September through June, precipitation begins in the study region. Therefore, the average precipitation for those months was determined. Since the soil samples were obtained in 2020, Table 2 displays the precipitation averages based on the hydrological years (1998–2021) (Gaznayee *et al.*, 2022).

2.2. Methodology

This research was completed in numerous main steps, including fieldwork, soil sampling, laboratory work (assessment of soil properties), remotely sensed dataset, statistical analysis, and utilizing significant relationships to model and map some soil properties of the study area shows a flowchart of the study methodology (Figure 2).

2.2.1. Field works

Data was gathered during the fieldwork for all soil sample locations, encompassing various aspects such as general soil conditions, topography, soil hardness, rock presence, slope, and plant species and types.

Additionally, photographs were captured at each location where soil samples were collected. The purpose of collecting this data was to conduct a comprehensive survey of the entire study area. Moreover, the fieldwork aimed to gather data specifically for interpreting satellite image features and conducting spectral analysis.

2.2.2. Soil sampling

A total of one hundred twenty georeferenced surface soil samples (0–25 cm) were collected from thirteen districts (Fig 1) and georeferenced. The GPS receiver (Garmin/Rino 530 HCx) was used to obtain each site's geographical information, including longitude, latitude, and elevation. The sampling took place between March and May of 2020. All collected soil samples were air-dried, crushed, and sieved through a 2-millimeter mesh to ensure uniformity and prepare them for analysis. Subsequently, the samples underwent a series of physical and chemical laboratory tests. However, only one

hundred twenty soil samples from the study area were subjected to spectral analysis. To store and manage the attribute data for the soil sample locations, a geodatabase was established within a GIS environment. Each of the 120 soil samples had forty records, encompassing various chemical and physical characteristics. The geodatabase served as the foundation for the entire interpolation procedure conducted in this study.

2.2.3. Laboratory works

Forty soil samples were subjected to several physical and chemical analyses, including particle size distribution (percentage of sand, silt, and clay) and air-dry soil moisture content. As the pH of the soil extract (1:1) was determined using a pH meter (Multiline P4/Set-2 following (Herrmann and Bucksch, 2014). The soil samples were subjected to chemical analysis. Based on Rowell (Herrmann and Bucksch, 2014), the EC of the soil extract (1:1) was measured using an EC meter (Multiline P4/Set-2) instrument. The organic matter was measured by oxidation using a solution of 1 mol of potassium dichromate $K_2Cr_2O_7$ in 95% sulfuric acid and calibration with 0.5 mol of ferrous ammonium sulfate and the Diphenylamine indicator (Herrmann and Bucksch, 2014), The soil's total calcium carbonate was determined using the titration technique (Mian, 2011).

The bicarbonate technique was used to quantify the available phosphorous, as described in (Parent *et al.*, 1993). Sodium was determined using the flame photometer technique described in (Parent *et al.*, 1993). Calcium and Magnesium were measured using the titration technique using EDTA as an indicator (Rowell, 1996(Herrmann and Bucksch, 2014)). In addition, spectral studies were done on representative soil samples from chosen research sites.

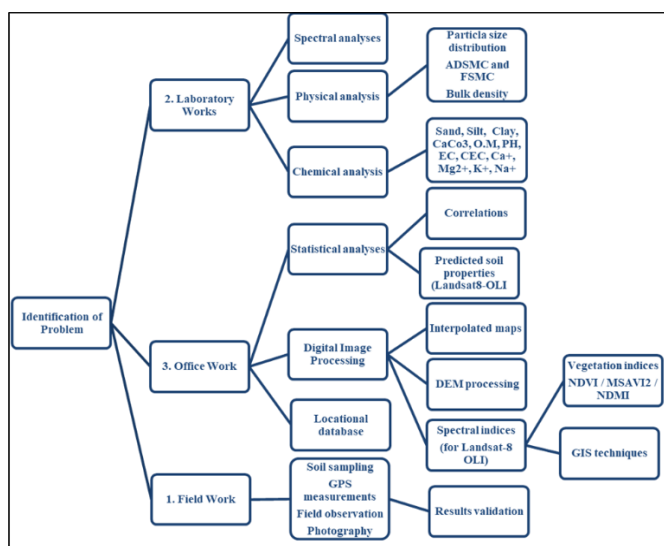


Fig 2: Flowchart of the applied methodology.

2.3. Remotely Sensed Dataset

2.3.1. Data collection

Two images of Landsat 8 OLI representing the data (168/35 and 168/36) for 2021 were assembled and used. The study year 2021 was chosen. A mosaic of two Landsat scenes was constructed for the year 2021. The imageries were downloaded from the United States Geological Survey (<https://ers.cr.usgs.gov/>) Landsat Collection 1 Surface Reflectance products delivered from EROS Science Processing Architecture On Demand Interface (ESPA). Landsat images were acquired in 2021, during which most vegetative proliferation occurred. Landsat images have a spatial resolution of 30 m. The Advanced Spaceborne Thermal Emission and Reflection Radiometer-Global Digital Elevation Model (ASTER-GDEM) V2 dataset with a spatial resolution of 30 m, available from the National Aeronautics and Space Administration (NASA; <https://www.nasa.gov/>), was utilized as the Digital Elevation Model (DEM) for this study (Fig. 1c); the DEM was used to identify the relationships between vegetation percentage and altitude. Daily and monthly precipitation datasets at the 22 meteorological stations in Sulaimaniyah Governorate were obtained from the Meteorological Department of the Ministry of Agriculture and Water Resources, Kurdistan Region Government (KRG), Iraq, during the period from 1998 to 2021. Detailed information on precipitation at the ten meteorological stations from 2000 to 2021 is shown in Table 2.

2.3.2. Spectral Vegetation Indices

Using the ArcGIS ver. 10.8.1, the vegetation spectral indices were calculated from Landsat OLI-8 images to emphasize and describe the vegetative cover in the study area. As spectral vegetation indices, this study employed the NDVI, MSAVI2, and NDMI. Then, the pixel reflectance values of all vegetation indices images were collected for 120 different sites to calculate their statistical relationships with the other study variables.

2.3.3. NDVI

The NDVI is the most used index for vegetation monitoring. It accounts for all the green vegetation and is based on the combination of red band and near infra-red (NIR) band wavelengths and can be computed by the well-known formula (Eq. 1) of (Rouse et al., 1974)

$$\text{NDVI} = (\text{NIR} - \text{RED}) / (\text{NIR} + \text{RED}), \text{ Eq. } (1)$$

where NDVI is the Normalized Difference Vegetation Index; NIR is the near infra-red band (850–880 nm), and RED is the red band (640–670 nm). Healthy vegetation has less reflection in the visible range of the electromagnetic spectrum (EMS) due to the absorption of chlorophyll and other pigments. However, it has a high reflectance in the NIR section of the EMS.

The NDVI is a strong vegetation signal and is mostly utilized to differentiate vegetative areas from non-vegetative areas (Huang and Shen, 2005). Its digital number values range from -1 to 1 . Specifically, values from -1 to 0 represent the non-vegetative features, such as bare surface, built-up area, and water bodies, while values from 0 to 1 represent vegetative cover features. (Al-Quraishi et al., 2021) are produced on-demand (using the USGS Earth Resources Observation and Science (EROS) Center Science Processing Architecture (ESPA) On Demand Interface).

2.3.4. MSAVI2

The Modified Soil Adjusted Vegetation Index (MSAVI) and its later revision, MSAVI2, are soil-adjusted vegetation indices that seek to address some of the limitations of NDVI when applied to areas with a high degree of exposed soil surface. Also, it was designed to reduce the influence of soil in the image and to enhance the

spectral sensitivity for concentrated vegetation cover.

whereas;

$$MSAVI2=(0.5)*\{2*(NIR+1)\sqrt{[(2*NIR+1)^2-8*(NIR-R)]}\} \text{ (Qi et al., 1994). Eq... (2)}$$

are produced on-demand, using the (USGS Earth Resources Observation and Science (EROS) Center Science Processing Architecture (ESPA) On Demand Interface).

2.3.5. NDMI

NDMI is used to determine vegetation water content. It is calculated as a ratio between the NIR and SWIR values in a traditional fashion (USGS, 2017).

$$(NIR - SWIR) / (NIR + SWIR) \text{ Eq... (3)}$$

$$\text{In Landsat 8, NDMI} = (\text{Band 5} - \text{Band 6}) / (\text{Band 5} + \text{Band 6}). \text{ Eq... (4)}$$

Landsat Surface Reflectance-derived NDMI are produced on-demand, (using the USGS Earth Resources Observation and Science (EROS) Center Science Processing Architecture (ESPA) On Demand Interface).

2.3.6. DEM

The DEM raster dataset of the study area was used to extract the elevation values of each of the forty sites with the ERDAS Imagine software. On the other hand, the DEM was processed and analyzed using ArcGIS 10.8 to produce the maps of the Aspect ratio. (Gaznayee; Al-Quraishi, 2019).

2.4. THE STATISTICAL ANALYSES

2.4.1. The Correlation Coefficient (r)

All variables in this study, including soil physical and chemical properties, Landsat-8 OLI image bands reflectance, all examined indices, and DEM-based elevation, had their correlation coefficients (r) computed. In addition, a correlation between observed and anticipated surface soil physicochemical parameters was done. (Pearson Correlation Coefficient) was chosen as the default approach for this purpose. To determine if two variables are connected, it is the usual practice to monitor how they change concurrently (Babbie and Benaquisto, 2009).

2.4.2. The Predicted maps of the soil properties

The anticipated maps for various surface soil attributes were created depending on the regression equations derived from the reflectance

of Landsat OLI8 bands. The regression equations to predict various soil qualities using some associated bands were applied to 000 ArcGIS 10.8 to generate a map of the correlated surface soil properties. They were then transferred to ArcMap for additional processing, which included the construction of pyramids and calculating statistics.

3. RESULTS & DISCUSSION

3.1. NDVI

The Landsat OLI-8 image underwent NDVI algorithm application to assess the status of vegetation cover. The results (refer to Figure 3) indicated that the total vegetation area covered 5176.3 square kilometers, accounting for 21.3% of the entire study area. These areas are presented in Table 3. The findings also revealed that the southwest and western parts of the study area had the lowest NDVI values, whereas the northeastern parts exhibited the highest values (Fig. 3). Figure 3 visually demonstrates the maximum and minimum values of NDVI, MSAVI2, and NDMI, which align with the fluctuations in NDMI values. In contrast, there are variations in precipitation averages across different locations (Fig. 1A). Some sites experienced high precipitation averages, leading to a positive impact on the increase in NDVI values (Fig. 3). Conversely, regions in the southwest of SU demonstrated decreased NDVI values and vegetation cover due to low precipitation and high temperatures during the growing seasons. It is worth noting that this reduction in precipitation is considered one of the main factors contributing to severe drought episodes in Iraq and its Kurdistan region, as observed in 2000 and 2008. These drought episodes were accompanied by a significant decline in moisture and organic matter (OM), as depicted in Figure 4.

3.2. MSAVI2

The percentage of land covered by vegetation was 5299.7 km² presented in Table 3. The vegetation indices results indicated that the vegetation cover density in the highest classes (high and moderate) was located in the northwest part of the study area. While it decreased gradually toward two directions; the South-East and the Southwest. Decreased vegetation cover can be linked to the climatic conditions of the study area. In more detail, the increase in rainfall averages causes an increase in the vegetation cover density. The low vegetation percentage may

have resulted from a mismatch between seasonal precipitation and plant needs during the evaluation of the critical growth stage. This result was also reported by (Al-Quraishi et al., 2021; Asam et al., 2018).

3.3.NDMI

Using the NDMI in the study area (Fig. 3), the distribution of soil/vegetation moisture was determined. The general trend showed a decrease in soil moisture from the North-East to the Southwest. This pattern aligns with the local climate conditions, particularly the variations in rainfall averages and temperature. The North-East parts experienced higher rainfall levels, averaging around 1,000 mm, which gradually decreased towards the Southwest parts, with an average of approximately 150 mm. Conversely, the temperature exhibited an inverse relationship compared to rainfall. The altitude followed a similar declining trend, indirectly influencing temperature and rainfall. Statistical analysis revealed a significant positive correlation between soil/vegetation moisture and the pixel values of the DEM. Conversely, there was a significant negative correlation with an area of 5825.1 square kilometers (24.0% of the study area) representing moist land pixel values (Table 3).

3.4. Interpolated maps for the measured soil properties

In general, there are several interrelations among the studied soil properties. The interpolated map represents a simulation of the spatial distributions of soil-measured properties. Therefore, this study attempted to plot some of the studied soil properties and find some relationships among those maps.

Table (3) The max, min, mean, std. dev. of MSAVI2 values and the area of vegetative cover

Indices	Vegetation Cover (Km ²)	Non-Vegetation Cover (Km ²)	Total Area (Km ²)
MSAVI2	5299.7	18996.3	24295.9
	%21.8	%78.2	
NDVI	5176.3	19119.6	24295.9
	%21.3	%78.7	
NDMI	Moistland	Dryland	
	5825.1	18460.9	24295.9
	%24.0	%76.0	

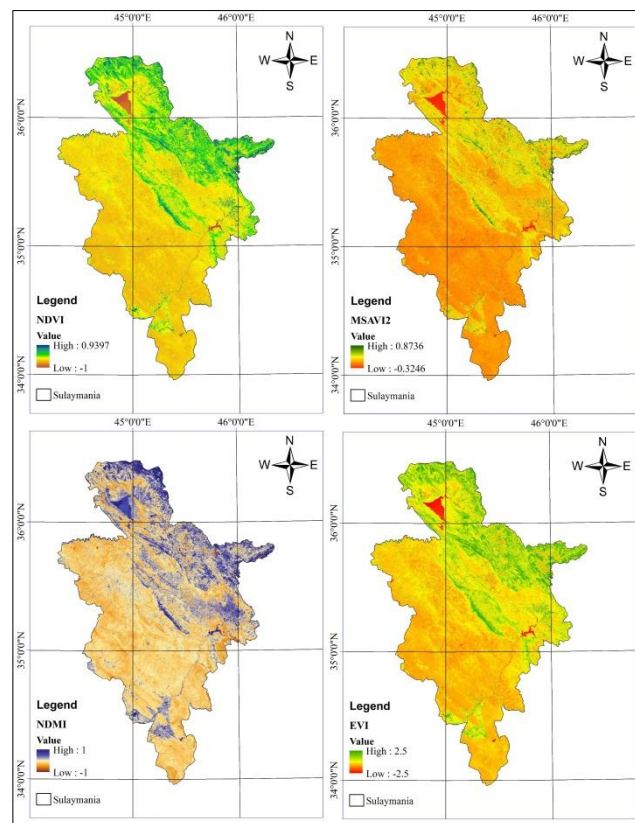


Fig 3: NDVI, MSAVI2, NDMI, and EVI Maps of the study area.

3.5. Soil physical properties

The following are the interpolated maps for the measured physical soil properties. The physical properties tested in the laboratory and their corresponding interpolated values were highly convergent, and the interpolated values on the maps were realistic and reliable. Figure 4 depicts the particle size distribution data for all sites, and a comparison of these results reveals several discrepancies in the clay, silt, and sand contents between soil sample locations. Their distribution pattern within a location reflects the effects of climate on that distribution. In Districts 8, 9, and 10, the clay content varied between 60 and 300 g kg⁻¹. All soil samples were taken from the surface layer (0–30 cm). In Districts 11,12,13,14 and 15, the range of clay levels was between 360 and 600 g kg⁻¹. The large amounts of total clay in some regions are mostly the result of geomorphic processes, specifically the transport and deposition of fine fractions that were changed from the surrounding highland soils to the low plain soils, hence increasing the clay content in that region.

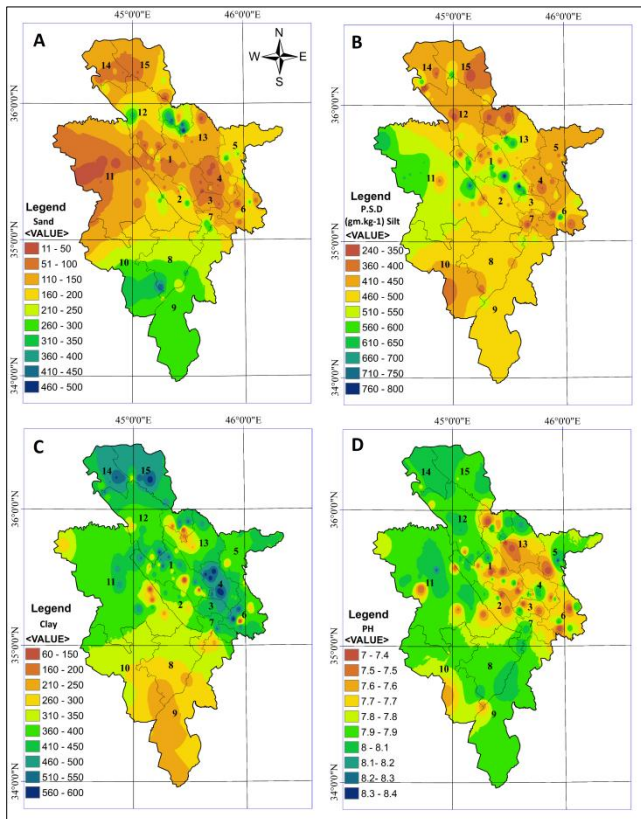


Fig 4: (A) Interpolated map of the measured sand in soil ;(B) Interpolated map of the measured Silt in soil (C) Interpolated map of the measured clay in soil, (D) and Interpolated map of the measured pH in soil.

3.6. Soil chemical properties

As shown below, the interpolated maps for the measured chemical soil properties were performed. As previously indicated, the observed chemical characteristics and their interpolated values were quite similar in this instance as well, and the interpolated values on the maps were accurate and may be relied upon when calculating the values for any location within the research region. The most significant CaCO_3 concentrations defined large portions of the southern Sulaimaniyah Governorate, while the majority of the rest of the study region was characterized by the lowest CaCO_3 concentrations (Fig. 5). The southern parts of the research area were warmer than the other regions. This large rise in CaCO_3 is attributable to the deficiency of OM, resulting in a moisture shortage and a smaller plant cover area on lands with low DEM (Fig. 1b and Fig. 6). CaCO_3 increases in the southeast and southwest of the research region led to a decline in CEC in the Sulaimaniyah Governorate. This indicates that increased CaCO_3 contributed significantly to decreasing NDVI, MSAVI2, NDMI, and EVI in the study area. Figure 4 illustrates the data regarding soil pH levels. The pH values

predominantly ranged from neutral to slightly alkaline, which can be attributed to the presence of calcareous parent material and environmental conditions. The results indicated pH variations between 7.0 and 8.0. Certain factors that influence soil pH, such as climate, CaCO_3 levels, and soil texture, cannot be easily modified.

Districts 1, 2, 3, 10, and 13 exhibited the lowest pH levels. Multiple factors contribute to this, including the composition of the parent material in those regions, higher concentrations of CO_2 , and the application of nitrogen. However, the exact extent of these factors' influence requires further investigation, as indicated by the significance level of $p < 0.05$ observed between the studied years. The relationship between NDMI, NDVI, and MSAVI2, as determined by a Pearson correlation analysis, is shown in Table 4 and Fig. 8. The correlation between vegetation indices and NDMI with O.M. and clay is statistically significant and negative. For each site, trends in chemical and physical properties have been determined. The majority of clay was located in the north and northeast. Fig. 4 depicts the findings of the trend analysis for sites 12, 14, 15, and 5. The correlation coefficients between Sand, Particle Size. The analysis of variance revealed significant differences between the variables at $p < 0.01$ and $p < 0.05$. The relationship between soil chemical, physical, and spectral indices, and the spectral band was analyzed using Pearson correlation, and the findings are shown in Table 6 and Fig 4, 5, and 6.

The results have noted that the observed chemical characteristics and their interpolated values were similar. The interpolated values on the maps are accurate and can be relied upon when calculating values for any location within the research region.

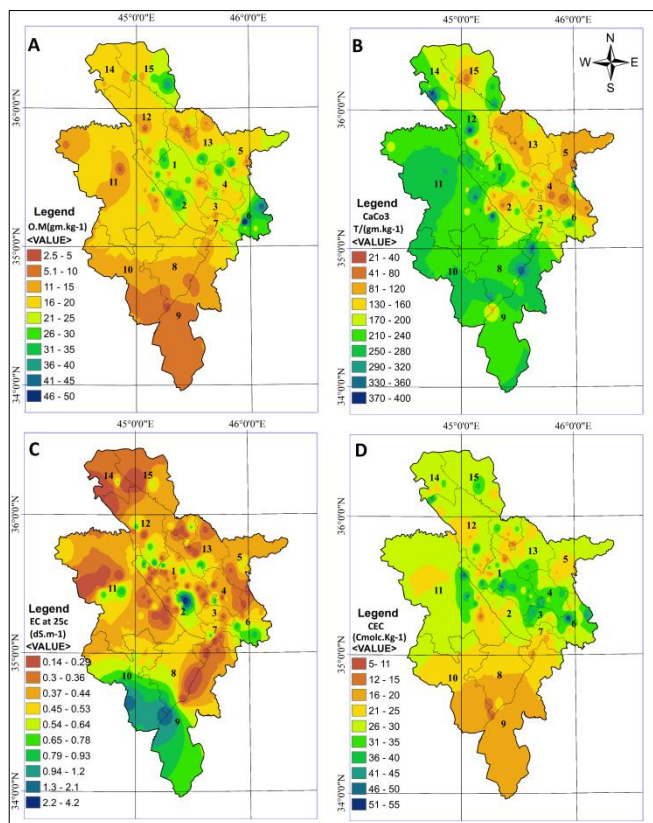


Fig 5: (A) Interpolated map of the measured Organic matter in soil, (B) Interpolated map of the measured CaCO₃ in soil, (C) Interpolated map of the measured EC in soil, and (D) Interpolated map of the measured CEC in soil.

The study results illustrate notable concentrations of CaCO₃ in substantial areas of the southern Sulaimaniyah Governorate, while the majority of the remaining study region exhibits low levels of CaCO₃. Furthermore, the findings indicate that the southern parts of the research area experience higher temperatures compared to other regions. In contrast, the proportion of total sand in Districts 11, 12, 13, 14, and 15 ranged from 11 to 200 g kg⁻¹. While the amount of total silt varied between 460 and 700 g kg⁻¹ in Districts 8, 9, 10, and 11, whilst the range was between 460 and 700 g kg⁻¹ in Districts 8, 9, 10, and 11. This vast variation might be due to the soil's sand-rich composition, which was generated by water erosion. In another location, similar variations may result from steep slopes and little plant coverage, and they result in the erosion of surface clay and silt particles and the elevation of a sand fraction.

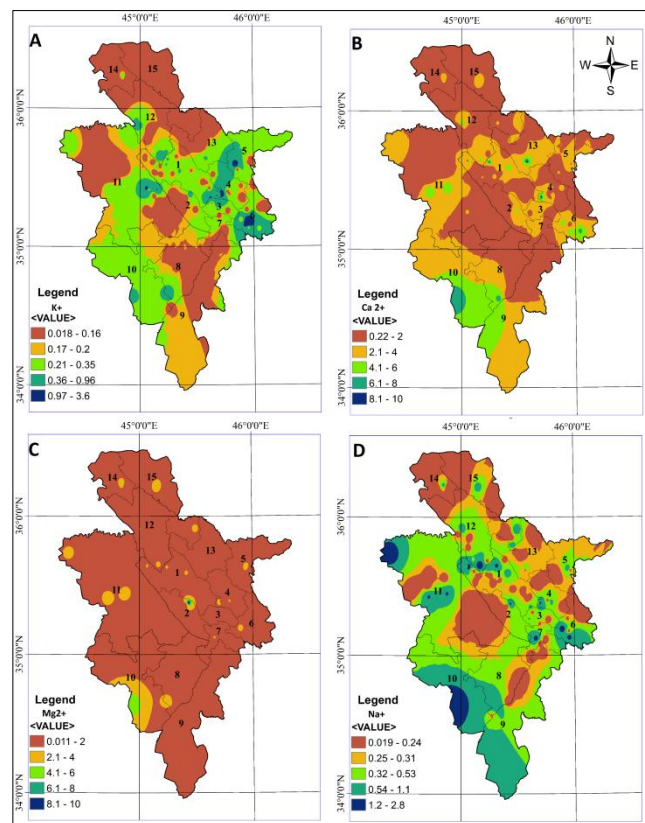


Fig 6: Interpolated map of the measured K in soil, Interpolated map of the measured Ca in soil, Interpolated map of the measured magnesium (Mg) in soil, and Interpolated map of the measured sodium ion (Na) in soil.

4. DISCUSSION

The study area has a vegetation distribution pattern that varies with geography, with the dense and moderately dense vegetation classes primarily located in the northwestern part of the area and decreasing towards the southeast and southwest. This pattern may be due to unfavorable climatic conditions for vegetation growth in the study area. Also, an increase in rainfall averages appears to encourage vegetation growth and density. This suggests that precipitation may be an important factor in determining the density of vegetation in the study area. It would be interesting to know more about the specific climatic conditions that may be limiting vegetation growth in the study area. For example, are there particular temperature ranges or soil types that are associated with lower vegetation density. Additionally, it would be useful to understand how the observed patterns of vegetation distribution have changed over time, and whether they are likely to continue changing in the future as a result of climate change or other factors. This

result was also is stated by Gaznayee (2021), and (Al-Quraishi, et al 2021).

Moreover, based on the DEM maps (Fig. 1), it is noticed that the elevation decreases coincide with the reduction of the vegetation cover density. The mountainous terrain is characterized by high elevation (around 2,000 meters above sea level). Generally, the IKR mountains are characterized by their great heights in the North and Northeastern parts, while their heights gradually decrease towards the South and Southwest. Statistical analysis showed significant positive correlations between the DEM values (elevations) and all vegetation indices. In more detail, NDVI appeared to have negative correlations with DEM, NDMI, and all studied vegetation indices. This trend explains that an increase in elevation causes a decrease in land surface temperature, which subsequently causes a rise in soil/vegetation moisture and offers a suitable local environment for vegetation growth.

The results also showed that MSAVI2 was the most vegetation index that highly responded to the aspect ratio than the other vegetation indices whereas MSAVI2-based vegetative cover extends between 35° Northwest and 46° northeast, as reported by (Jin et al., 2008). The aspect ratio results disclosed that the maximum growth of the vegetation cover was at the shaded side of the mountains in the study area more than on the sunny side, whereas denser vegetation cover was noticed on the shady side. On the contrary, much less evapotranspiration is expected, which is essential for vegetation growth, and is mainly noticed when the mountains are located in a semiarid region (Jin et al., 2008). In terms of OM (Fig. 5), it is evident that the vegetation cover presence is positively related to the vegetation. From the northeast to the Southwest direction, the CaCO₃ increase was obvious, concomitant with diminishing vegetation cover (Fig. 3). Several environmental factors control vegetation cover growth and its spatial distribution, such as topographical factors and their influence on climate conditions (Kapoor, 2020). Statistically, the results revealed a Positive significant correlation between NDMI values and all vegetation indices, as previously mentioned in this paper. Gillie, (2010) stated that the relationship between soil moisture, and NDVI, could be called a “Universal Triangle”. Furthermore, elevation, aspect, and slope are the main topographic factors controlling vegetative cover distribution in mountainous areas (Gillies, 2010). Among the

various vegetation indices utilized in this study, it was found that the Clay index (Table 3) detected a larger vegetative area in the study region, indicating its greater sensitivity to vegetation compared to the other indices. However, the MSAVI2 index emerged as the most reliable and efficient indicator for detecting sparse vegetation. The validation of our study results confirmed the effectiveness of the studied vegetation indices in mapping vegetation presence and vitality across different sites within the study area. Furthermore, our findings revealed that the MSAVI2 index exhibited the strongest association with changes in aspect ratio and slope. Li et al. (Jin et al., 2008) also found that MSAVI2 is a very good vegetation index that was made to reduce the effect of soil on the image and increase spectral sensitivity for dense vegetation.

These sensors-based indices detected various wavelengths of electromagnetic radiation, which can be used to identify different features on the earth's surface, including soil properties. Multivariate statistical analyses, on the other hand, involve the use of statistical models to analyze data from multiple variables. By combining remote sensing and multivariate statistical analyses. One of the key advantages of this research is its ability to provide soil data at a large spatial scale, which can be particularly useful for mapping soil properties in remote or inaccessible areas. It can also be used to monitor changes in soil properties over time, providing valuable information for land management and environmental monitoring. On the other side, predicting and digital mapping surface soil properties using remote sensing and multivariate statistical analyses is a powerful technique that can revolutionize soil mapping and monitoring for physical and Chemical properties. As remote sensing technology improves and becomes more accessible, this technique is likely to become even more valuable for a wide range of applications.

Table (4) Correlation matrix (Pearson): between Spectral indices, band, and Soil Properties.

Variables	b1	b2	b3	b4	b5	b6	b7	sand	PSD	Clay	Caco3	O_M	PH	Ec	CEC	Ca	Mg2	K	Na	VI	NDMI	NDVI	MSAVI2
b1	1.00	0.99	0.96	0.94	0.62	0.81	0.87	0.30	0.21	-0.47	0.45	-0.39	0.01	0.32	-0.32	0.35	0.21	0.01	0.29	-0.62	-0.48	-0.69	-0.61
b2	0.99	1.00	0.99	0.96	0.67	0.83	0.87	0.28	0.22	-0.44	0.43	-0.36	-0.01	0.33	-0.29	0.34	0.21	0.03	0.29	-0.61	-0.45	-0.68	-0.60
b3	0.96	0.99	1.00	0.98	0.72	0.86	0.88	0.28	0.22	-0.45	0.44	-0.35	-0.01	0.33	-0.29	0.35	0.22	0.05	0.29	-0.58	-0.43	-0.66	-0.56
b4	0.94	0.96	0.98	1.00	0.74	0.90	0.91	0.26	0.24	-0.43	0.44	-0.34	0.00	0.31	-0.27	0.33	0.20	0.07	0.28	-0.58	-0.48	-0.65	-0.56
b5	0.62	0.67	0.72	0.74	1.00	0.78	0.62	0.20	0.09	-0.26	0.16	-0.15	-0.11	0.26	-0.14	0.24	0.15	0.08	0.17	0.10	0.03	-0.01	0.13
b6	0.81	0.83	0.86	0.90	0.78	1.00	0.94	0.20	0.26	-0.39	0.38	-0.30	-0.04	0.27	-0.23	0.28	0.17	0.08	0.24	-0.40	-0.56	-0.46	-0.37
b7	0.87	0.87	0.88	0.91	0.62	0.94	1.00	0.22	0.30	-0.44	0.47	-0.35	0.01	0.27	-0.26	0.30	0.19	0.06	0.27	-0.57	-0.66	-0.61	-0.56
sand	0.30	0.28	0.28	0.26	0.20	0.20	0.22	1.00	-0.39	-0.75	0.17	-0.47	-0.02	0.56	-0.72	0.49	0.27	0.03	0.35	-0.12	-0.09	-0.14	-0.12
PSD	0.21	0.22	0.22	0.24	0.09	0.26	0.30	-0.39	1.00	-0.31	0.34	-0.09	-0.05	-0.15	0.08	-0.14	-0.23	0.02	-0.10	-0.25	-0.21	-0.26	-0.24
Clay	-0.47	-0.44	-0.45	-0.43	-0.26	-0.39	-0.44	-0.75	-0.31	1.00	-0.42	0.55	0.06	-0.47	0.69	-0.40	-0.11	-0.05	-0.29	0.30	0.24	0.32	0.30
Caco3	0.45	0.43	0.44	0.44	0.16	0.38	0.47	0.17	0.34	-0.42	1.00	-0.48	0.39	0.14	-0.40	0.19	0.10	-0.09	0.25	-0.44	-0.35	-0.45	-0.44
O_M	-0.39	-0.36	-0.35	-0.34	-0.15	-0.30	-0.35	-0.47	-0.09	0.55	-0.48	1.00	-0.29	-0.35	0.62	-0.40	-0.24	0.31	-0.36	0.29	0.20	0.30	0.29
PH	0.01	-0.01	-0.01	0.00	-0.11	-0.04	0.01	-0.02	-0.05	0.06	0.39	-0.29	1.00	-0.25	-0.22	-0.23	-0.15	-0.28	-0.13	-0.12	-0.06	-0.10	-0.12
Ec	0.32	0.33	0.33	0.31	0.26	0.27	0.27	0.56	-0.15	-0.47	0.14	-0.35	-0.25	1.00	-0.40	0.84	0.71	0.24	0.68	-0.14	-0.08	-0.17	-0.14
CEC	-0.32	-0.29	-0.29	-0.27	-0.14	-0.23	-0.26	-0.72	0.08	0.69	-0.40	0.62	-0.22	-0.40	1.00	-0.32	-0.12	0.16	-0.24	0.21	0.16	0.22	0.21
Ca	0.35	0.34	0.35	0.33	0.24	0.28	0.30	0.49	-0.14	-0.40	0.19	-0.40	-0.23	0.84	-0.32	1.00	0.77	0.32	0.85	-0.18	-0.10	-0.20	-0.18
Mg2	0.21	0.21	0.22	0.20	0.15	0.17	0.19	0.27	-0.23	-0.11	0.10	-0.24	-0.15	0.71	-0.12	0.77	1.00	0.29	0.85	-0.11	-0.06	-0.12	-0.11
K	0.01	0.03	0.05	0.07	0.08	0.08	0.06	0.03	0.02	-0.05	-0.09	0.31	-0.28	0.24	0.16	0.32	0.29	1.00	0.28	-0.01	0.00	-0.01	0.00
Na	0.29	0.29	0.29	0.28	0.17	0.24	0.27	0.35	-0.10	-0.29	0.25	-0.36	-0.13	0.68	-0.24	0.85	0.85	0.28	1.00	-0.20	-0.15	-0.21	-0.20
VI	-0.62	-0.61	-0.58	-0.58	0.10	-0.40	-0.57	-0.12	-0.25	0.30	-0.44	0.29	-0.12	-0.14	0.21	-0.18	-0.11	-0.01	-0.20	1.00	0.74	0.98	1.00
NDMI	-0.48	-0.45	-0.43	-0.48	0.03	-0.56	-0.66	-0.09	-0.21	0.24	-0.35	0.20	-0.06	-0.08	0.16	-0.10	-0.06	0.00	-0.15	0.74	1.00	0.69	0.74
NDVI	-0.69	-0.68	-0.66	-0.65	-0.01	-0.46	-0.61	-0.14	-0.26	0.32	-0.45	0.30	-0.10	-0.17	0.22	-0.20	-0.12	-0.01	-0.21	0.98	0.69	1.00	0.97
MSAVI2	-0.61	-0.60	-0.56	-0.56	0.13	-0.37	-0.56	-0.12	-0.24	0.30	-0.44	0.29	-0.12	-0.14	0.21	-0.18	-0.11	0.00	-0.20	1.00	0.74	0.97	1.00

5. CONCLUSIONS

In this study, we investigated and compared the performance of Two spectral vegetation indices and One land spectral index in the study area in the Sulaimaniyah. The results revealed that chemical and Physical properties could be considered reliable, and efficiently utilized to explore the vitality and existence of vegetative cover in the semi-area. Besides, the results revealed that dense vegetation is spreading in the Northwest part of the study area and gradually decreasing toward the South and Southeastern parts.

Vegetation shrinkage could be ascribed to decreasing elevation and rain amounts associated with an increase in land surface temperature and decreased OM, PH, Clay, and CEC.

An elevation increase could reduce surface temperature associated with rain amounts increase, which consequently offers suitable conditions for dense vegetation growth and existence. However, this study's results could support future work to incorporate soil.

Vegetation Indices obtained from remote sensing-based canopies are quite simple and effective algorithms for quantitative and qualitative evaluations of vegetation cover, vigor, and growth dynamics, among other applications.

Remote sensed information about terrestrial vegetation growth, vigor, and dynamics can provide beneficial insights for environmental monitoring, biodiversity conservation, agriculture, forestry, urban green infrastructures, and other fields.

Specifically, these types of information applied to agriculture provide not only an objective basis (depending on resolution) for the macro and micro-management of agricultural production but also in many occasions, the necessary information for yield estimation of crops (Xue and Su, 2017).

1. All of the studied vegetation indices indicated that the vegetation cover was denser in the study area in North-West and gradually decreased into two directions: South-East and Southwest.

2. The elevation was one of the important factors affecting this study's variables, especially the vegetation cover. As well as, the derived maps from the DEM, Chemical, and physical properties also had the same importance for the dissection of the distribution of the vegetation cover in the study area.

3. Most soil's physical and chemical properties had statistically solid relationships with Landsat 8OLI-based bands reflectance.

4. The wavelengths (bands) reflectance with the soil's physical and chemical properties had statistical strong relationships.

5. The predicted soil properties maps were generated using Kriging Interpolation.

Acknowledgements

This study was supported by the University of Salahaddin Erbil/Iraq. The authors would like to thank the United States Geological Service (USGS) for providing the Landsat images freely, Ministry of Agriculture and Water Resources in KRI/ General Directorate of Water Resources, Salahaddin University, and the Tishk International University, Erbil, Kurdistan Region, Iraq, for their valuable support. The Author acknowledges with many thanks to Mr. Peshawa Barzan.

We are also thankful to Sulaimaniyah University.

Conflict of Interest (1)

References

- ABUELGASIM, A., AMMAD, R., 2019. Mapping soil salinity in arid and semi-arid regions using Landsat 8 OLI satellite data. *Remote Sens. Appl. Soc. Environ.* 13, 415–425.
- AHMED, H.A., AL-QURAIISHI, A.M.F., 2020. Drought Trend Analysis in Sulaimaniyah, the Iraqi Kurdistan Region using Remote Sensing and GIS for a Period of 1998-2017.
- AKBARI, M., GOUDARZI, I., TAHMOURES, M., ELVENY, M., BAKHSHAYESHI, I., 2021. Predicting soil organic carbon by integrating Landsat 8 OLI, GIS and data mining techniques in semi-arid region. *Earth Sci. Informatics* 14, 2113–2122.
- AL-QURAIISHI, A., RAZVANCHY, H., GAZNAYEE, H.A.A., 2020. A Comparative Study for Performance of Five Landsat-based Vegetation Indices: Their Relations to Some Ecological and Terrain Variables. *J. Geoinformatics Environ. Res.* 1, 20–37.
- AL-QURAIISHI, A.M.F., GAZNAYEE, H.A., CRESPI, M., 2021. Drought trend analysis in a semi-arid area of Iraq based on Normalized Difference Vegetation Index, Normalized Difference Water Index and Standardized

- Precipitation Index. *J. Arid Land* 13, 413–430.
- AL-QURAIISHI, A.M.F., NEGM, A.M., 2019. Environmental Remote Sensing and GIS in Iraq, Springer.
- AL-QURAIISHI, A.M.F., SADIQ, H.A., MESSINA, J.P., 2019. Characterization and modeling surface soil physicochemical properties using Landsat images: A case study in the Iraqi Kurdistan region. *Int. Arch. Photogramm. Remote Sens. Spat. Inf. Sci. - ISPRS Arch.* 42, 21–28.
- ASAM, S., CALLEGARI, M., MATIU, M., FIORE, G., DE GREGORIO, L., JACOB, A., MENZEL, A., ZEBISCH, M., NOTARNICOLA, C., 2018. Relationship between Spatiotemporal Variations of Climate, Snow Cover and Plant Phenology over the Alps—An Earth Observation-Based Analysis. *Remote Sens.* 10, 1757.
- BABBIE, E.R., BENAQUISTO, L., 2009. Fundamentals of social research. Cengage Learning.
- ESKANDARI DAMENEH, H., GHOLAMI, H., TELFER, M.W., COMINO, J.R., COLLINS, A.L., JANSEN, J.D., 2021. Desertification of Iran in the early twenty-first century: assessment using climate and vegetation indices. *Sci. Rep.* 11, 1–18.
- GAZNAYEE, H.A. A; AL-QURAIISHI, A.M.F., 2019. Analysis of agricultural drought, rainfall, and crop yield relationships in erbil province, the kurdistan region of iraq based on landsat time-series msavi2. *J. Adv. Res. Dyn. Control Syst.* 11, 536–545.
- GAZNAYEE, H.A.A., AL-QURAIISHI, A.M.F., MAHDI, K., RITSEMA, C., 2022. A Geospatial Approach for Analysis of Drought Impacts on Vegetation Cover and Land Surface Temperature in the Kurdistan Region of Iraq. *Water* 14, 927.
- HARTEMINK, A.E., 2016. The definition of soil since the early 1800s. *Adv. Agron.* 137, 73–126.
- HAYES, D.J., COHEN, W.B., 2007. Spatial, spectral and temporal patterns of tropical forest cover change as observed with multiple scales of optical satellite data. *Remote Sens. Environ.* 106, 1–16.
- HERRMANN, H., BUCKSCH, H., 2014. Soil Science, Dictionary Geotechnical Engineering/Wörterbuch GeoTechnik.
- HUANG, N.E., SHEN, S.S.P., 2005. Hilbert-huang transform and its applications. *Hilbert-huang Transform Its Appl.* 1–311.
- JIN, X.M., ZHANG, Y.-K., SCHAEPMAN, M.E., CLEVERS, J.G.P.W., SU, Z., 2008. Impact of elevation and aspect on the spatial distribution of vegetation in the Qilian Mountain area with remote sensing data. *Int. Arch. Photogramm. Remote Sens. Spat. Inf. Sci. - ISPRS Arch.* 37, 1385–1390.
- KAPOOR, L.D., 2020. Botanical Studies. *Opium Poppy* 11, 19–40.
- KERCIVAL, N., 2015. Assessing Changes in Land Use and Land Cover using Remote Sensing: A Case Study of the Umhlanga Ridge Sub-Place.
- LUTES, D.C., KEANE, R.E., CARATTI, J.F., KEY, C.H., BENSON, N.C., SUTHERLAND, S., GANGI, L.J., 2006. FIREMON: Fire effects monitoring and inventory system. Gen. Tech. Rep. USDA Forest Service RMRS-GTR-164-CD. USDA For. Serv. - Res. Pap. 410.
- MIAN, I.A., 2011. Characterization of Rod Kohi Soils Of D. I. Khan, Pakistan Citation : 27, 27–30.
- NAJMADDIN, P.M., WHELAN, M.J., BALZTER, H., 2017. Estimating daily reference evapotranspiration in a semi-arid region using remote sensing data. *Remote Sens.* 9.
- NANNI, M.R., DEMATTÊ, J.A.M., CHICATI, M.L., FIORIO, P.R., CÉZAR, E., DE OLIVEIRA, R.B., 2012. Informações espectrais de imagens landsat da superfície do solo como indicativo na discriminação de classes de solos. *Acta Sci. - Agron.* 34, 103–112.
- NAWAR, S., BUDDENBAUM, H., HILL, J., 2015. Digital mapping of soil properties using multivariate statistical analysis and ASTER data in an Arid region. *Remote Sens.* 7, 1181–1205.
- PARENT, L.E., CARON, J., CARTER, M.R., 1993. Physical properties of organic soils. *Soil Sampl. methods Anal.* 441–458.
- QADER, S.H., DASH, J., ALEGANA, V.A., KHWARAHM, N.R., TATEM, A.J., ATKINSON, P.M., 2021. The role of earth observation in achieving sustainable agricultural production in arid and semi-arid regions of the world. *Remote Sens.* 13, 1–27.
- QI, J., CHEHBOUNI, A., HUETE, A.R., KERR, Y.H., SOROOSHIAN, S., 1994. A modified adjusted vegetation index (MSAVI). *Remote Sens. Environ.* 48, 119–126.
- R. R. GILLIES, W.P.K. & K.S.H., 2010. A verification of the 'triangle' method for obtaining surface soil water content and energy fluxes from remote measurements of the Normalized Difference Vegetation Index (NDVI) and surface e. *Int. J. Remote Sens.* 37–41.

- RAZVANCHY, H.A.S., 2008. Modelling Some of the Soil Properties in the Iraqi Kurdistan Region using Landsat Datasets and Spectroradiometer.
- RED, N., 2006. List of Vegetation Spectral Indices References Baret, F., G. Guyot, and D. Major. 1989. TSAVI: a vegetation index which minimizes soil brightness effects on LAI and APAR estimation. 12th Canadian Symposium on Remote Sensing and IGARSS '90, p. Remote Sens. Environ. 1994–1996.
- ROUSE, J.W., HAAS, R.H., SCHELL, J.A., DEERING, D.W., HARLAN, J.C., 1974. Monitoring the vernal advancements and retrogradation of natural vegetation. NASA/GSFC, Final Report, Greenbelt, MD, USA 1–137.
- SENANAYAKE, S., PRADHAN, B., HUETE, A., BRENNAN, J., 2020. A review on assessing and mapping soil erosion hazard using geoinformatics technology for farming system management. *Remote Sens.* 12, 1–25.
- SHABOU, M., MOUGENOT, B., CHABAANE, Z.L., WALTER, C., BOULET, G., AISSA, N. BEN, ZRIBI, M., 2015. Soil clay content mapping using a time series of Landsat TM data in semi-arid lands. *Remote Sens.* 7, 6059–6078.
- USGS, 2017. Product guide 1–14.
- VAUDOUR, E., COSTANTINI, E., JONES, G. V., MOCALI, S., 2015. An overview of the recent approaches to terroir functional modelling, footprinting and zoning. *Soil* 1, 287–312.
- VICENTE BARROS AND CHRISTOPHER B. FIELD, 2012. Managing the Risks of Extreme Events and Disasters to Advance Climate Change Adaptation.
- WODAJE, S.T., 2016. Land Degradation Vulnerability Assessment Using GIS and Remote Sensing in Beshilo River Basin, Ethiopia 1–81.
- XUE, J., SU, B., 2017. Significant remote sensing vegetation indices: a review of developments and applications. *J. sensors* Vol.2017, 17p.
- YAGHOUBI, A., ZARGAR, H., 2012. Handling Uncertainty In Hydrologic Analysis and Drought Risk Assessment 154.